INVESTIGATION OF THE PLANETARY BOUNDARY LAYER HEIGHT VARIATIONS OVER COMPLEX TERRAIN

R. LIEMAN and P. ALPERT
Tel-Aviv University, Tel-Aviv, Israel.

(Received October 1991)

Abstract. The effects of sea-breeze interactions with synoptic forcing on the PBL height over complex terrain are investigated through the use of a 3-D mesoscale numerical model. Two of the results are as follows. First, steep PBL height gradients – order of 1500 m over a grid interval of 10 km – are associated with the sea-breeze front and are enhanced by the topography. Second, a significant horizontal shift in the maximum PBL height relative to the mountains, is induced by a corresponding displacement of the thermal ridge due to the mountains, in the presence of large scale flow.

1. Introduction

The realistic distributions of planetary boundary layer (PBL) heights over complex topography are of particular importance for a good prediction of the dispersion of air pollutants. Observational studies by radiosondes/minisondes (Dayan *et al.*, 1988) and recently also by lidar (laser-radar), e.g. Hasmonay *et al.* (1990) are of limited value over complex terrain because of the relatively large expected spatial variance of PBL height. In contrast, the analytical studies focus mostly on flat terrain, e.g. Stull (1988), and the main tool over complex terrain remains the three dimensional (3-D) numerical model, e.g. Anthes and Warner (1978), Segal *et al.* (1982,1985), Alpert and Getenio (1988) and Alpert *et al.* (1988). The 3-D models, however, became quite expensive to operate particularly when high horizontal and vertical resolutions are required, e.g. Seaman *et al.* (1989), and therefore relatively few such experiments have been performed over the meso-$\tilde{A}$ scale ($\check{S}_x \sim 5 - 10\ km$). Also, these studies focused mostly on the flow fields, and less on PBL height variations (Alpert, 1988).

Hence, the purpose of the present study is to focus on the temporal and spatial variations of the convective PBL height in association with the relevant dynamical processes over complex terrain. For this, a 3-D high resolution mesometeorological model was applied over Israel for two realistic cases with opposing geostrophic flow and different synoptic situations. One is a warm summer case with a generally onshore westerly current, while the other is a cold winter case with an easterly offshore current (not shown in detail in this work).

Boundary-Layer Meteorology **62:** 129–142, 1993.

2. Model and Method

2.1. Model and Mesh

The recent MM4 version of the PSU/NCAR mesoscale model as described by Anthes and Warner (1978) and Anthes *et al.* (1987) was applied over a region of 300x360 km in the southeast Mediterranean, Fig. 1, with horizontal resolution of $\check{S}x = \check{S}y = 10\ km$. The vertical coordinate is a normalized pressure $\bar{I}$ and the model has 16 $\bar{I}$-levels whose altitudes above the ground are approximately given by: 0, 20, 40, 80, 160, 320, 640, 1280, 2000, 13000, 4000, 6000, 8000, 10000, 12000 and 16000 m. The model equations and the numerical schemes are reviewed by Anthes *et al.* (1987). The present simulations were carried out without moisture and could be partly justified by the clear and relatively dry events that have been chosen.

2.2. Initalization

The static initialization – e.g., Haltiner and Williams (1980) –was chosen since it was found that the model adjustment to strong local forcings, thermal as well as topographical, were quite fast. The Cressman (1959) interpolation over isobaric surfaces was performed adopting the Goodin *et al.* (1979) radius of influence R,

$$R = 1.66\sqrt{A/N} \tag{1}$$

where A is the area of the large-domain, see Fig. 1, and N the number of available radiosondes. The variables were then vertically interpolated to the $\bar{I}$-levels and the vertically averaged divergence of the horizontal wind was required to vanish. This was done in order to prevent initial gravity wave disturbances, e.g. Pielke (1984). Six neighbouring radiosondes were used for the initialization in successive applications of the Cressman interpolation (more details are found in Lieman,1990).

The model was quite sensitive to the lateral boundary conditions and following a few experiments, the sponge boundary condition was applied with a varying boundary weight for the synoptic large-scale flow increasing gradually from 1 at the boundary to 0 at the fifth inner domain point.

2.3. Surface Properties

Table I summarizes some of the surface parameters for our simulations. The surface temperature is calculated through a surface thermal energy balance following Deardorff (1978).

2.4. Model Topography

Envelope orography was used, where the standard deviation of the topographical height as calculated over 1 km horizontal resolution, was added to the average altitude at each point. Since the simulation grid interval was 10 km, 100 points were involved in the calculation for each point. The resulting topography along with surface stations used for model verifications are shown in Fig. 2, which

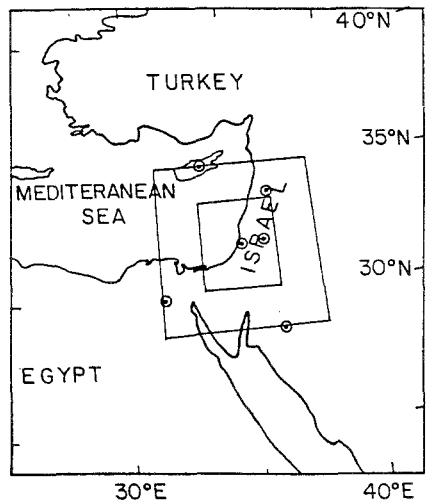

Fig. 1. General view of the area. The large-domain for the initialization and the smaller domain illustrating the simulation area. The available radiosondes are indicated by ⊙.

TABLE I
Surface properties in the model simulations

	Albedo	Soil Moisture (%)	Roughness Length (cm)	Soil heat capacity (cal $cm^2 K^{-1} sec^{-0.5}$)	Emissivity at 9 μ in (%)
Land	0.25	2-5	10	0.02	85
Sea	0.08	100	10^{-4}	0.06	98

shows two major north to south mountain ranges at distances of about 40 and 100 km from the Mediterranean coast respectively. Fig. 3 shows the west to east topographical cross-section along 32°N (ordinate 21 in Fig. 2) with and without the envelope orography along with the original topography based on the 1 km resolution. In order to find the optimal horizontal grid interval which captures most of the topographical variance, the cross-section height function (Fig. 3) was decomposed into its Fourier components, following the suggestion by Young and Pielke (1983). From the distribution of topographical variance as a function of wavelength, one finds that a 10 km interval represents the major part (over 95%) of the variance based on the 1 km resolution. A considerable reduction in the topographical variance occurs when the grid interval doubles to only 20 km. This result led to our decision to use a 10 km grid interval.

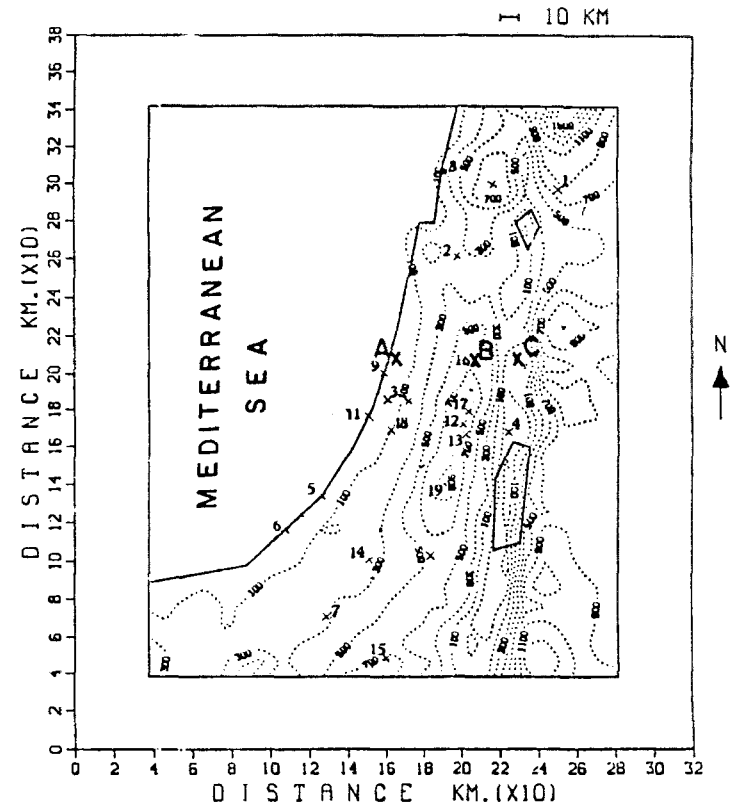

Fig. 2. Model topography with contour interval of 200 m. The surface stations used for model verification are indicated. Points A, B and C are referred to later.

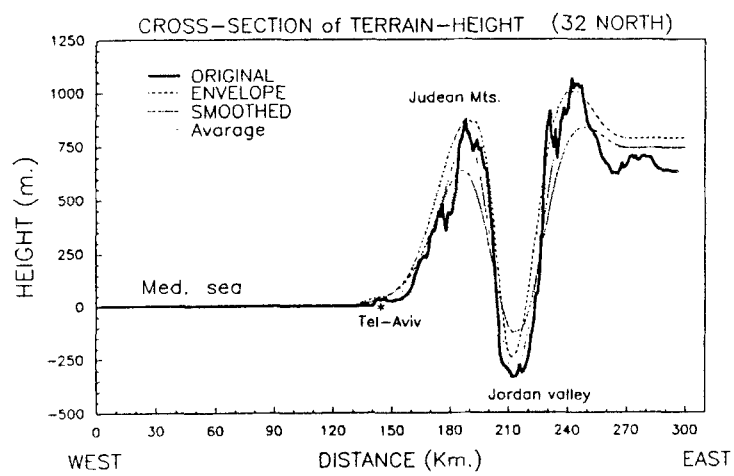

Fig. 3. Topographical cross-section along latitude 32°N (full) by 1 km resolution. The other lines are with 10 km resolution representing: (i) simple average by 10 points (dotted); (ii) as in (i) with smoothing (dashed-dotted); and (iii) as in (i) with the addition of the standard deviation to obtain envelope orography (dashed).

2.5. PBL HEIGHT

The turbulent fluxes in the PBL are calculated through the high resolution parameterization of Zhang and Anthes (1982), who follow the Blackadar (1977) formulation. The study focuses on events with clear days and strong solar radiation so that the two convection criteria are met. These are:

i) $h/L > 1.5$

ii) $Ri_b < 0$

where h is the PBL height, L the Monin-Obukhov length and Ri_b is the bulk Richardson number. Fig. 4 illustrates the vertical structure of the 1-D PBL model, where Z_1 is top of surface layer, Z_2, Z_3, Z_4 etc., are the higher PBL levels at the aforementioned model altitudes, Θ_{vg}, Θ_{va}, are the virtual potential temperatures of the ground surface and the lowest model level respectively. The PBL height h is then calculated through the thermodynamic approach by comparing the positive (P) to the negative (N) buoyancy regions, see Fig. 4. The height h defined in this manner is slightly higher than the zero buoyancy height or the level of most negative heat flux (other definitions that are commonly used for defining the mixed-layer height). The current approach does not neglect the turbulent entrainment at the top of the PBL, but assumes a constant entrainment coefficient (E=0.2) as discussed in Anthes *et al.* (1987). Stull (1988) pointed out that this turbulent entrainment accounts for about 10-20% of the observed variation of the mixed-layer depth.

3. Model Results –Summer Case

3.1. SYNOPTIC BACKGROUND

During summer, the eastern Mediterranean is dominated by a Subtropical ridge extending from the north-African shores to the east, and by the Persian trough extending from the monsoonal low through the Persian Gulf to the northeast Mediterranean and Turkey, e.g. Alpert *et al.* (1991). Fig. 5a, b show the 1000 and 500 HPa ECMWF analyzed charts for such a typical summer case on the 17 June 1987, 12 UTC. The Persian trough induced a northerly-northwesterly synoptic near-surface wind flow (Fig. 5a,5b) slightly weaker than the summer average along with a 500 HPa (not shown) upper-level weak trough to the east. Fig. 6 shows the vertical cross-section along latitude 32° N based on the ECMWF initialized dataset showing significant downward motion due to upper-level subsidence. The downward motion which persists through the summer is believed to be responsible for the quite steady inversion or stable layer found at an average altitude of 764 m (Dayan *et al.*, 1988). Although the Bet-Dagan radiosonde for 17 June 1987 12 UTC (14 LST), Fig. 7, does not show the common summer inversion, a relatively stable layer (1000-2000 m) can be noticed which is associated typically with drier air aloft the mixed layer. It was a clear sunny day with near-surface maximum temperatures of 29-30°C.

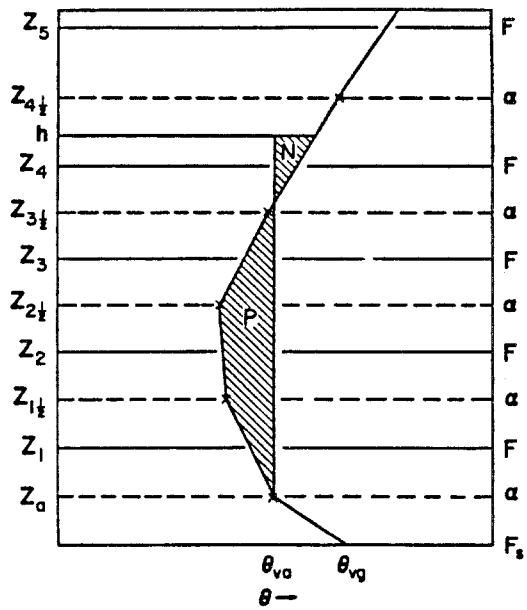

Fig. 4. The vertical structure of the 1-D PBL model where Z_1 is top of the surface layer, Z_2, Z_3, Z_4 etc. are the higher PBL model levels. The virtual potential temperatures of the ground and the lowest model level are Θv_g, Θv_a respectively. The shaded regions P and N represent positive and negative buoyancy layers respectively, that are associated with a parcel of air originating at z rising to h, the top of the PBL. Prognostic variables denoted by $\tilde{A}$ are calculated at half-levels (surface, 1.5, 2.5...) while fluxes (F) are computed at the levels 1,2 etc. For further details see Anthes *et al.* (1987).

3.2. MODEL SIMULATION

The simulation started on 06 UTC, and the large thermal forcing at this time led to a relatively short adjustment period (Segal *et al.*, 1985) of only about a couple of hours. Fig. 8a shows the surface winds after 6h, at 12 UTC, indicating that the eastern Mediterranean (EM in brief) region is dominated by a westerly-northwesterly 5-7 m/s flow as observed, (the observed wind vectors are also shown), see Segal *et al.* (1985), Alpert (1988). Above the mountain ridges winds accelerate to about 10 m/s and are associated with the major growth of the PBL height up to about 3000 m as indicated by the h isolines. The upper level PBL flow at 925 HPa –about 750 m above MSL or 100-200 m above the western mountain ridge –shows stronger winds above the mountain ridge; these winds are enhanced by the sea-breeze (SB) front. The SB front is typified by a relatively sharp horizontal temperature gradient (Fig. 8b), and even more interesting is the very sharp drop of the PBL height from 3000 m to less than half (1500 m) through a distance of only one grid point –10 km. To the south, the horizontal PBL height gradient is smaller, and is probably associated with the weaker SB due to the gentler topographic slopes in the south as well as the increased distance of the mountains from the coastline. Some boundary effects cannot be ruled out as well. Another factor enhancing the

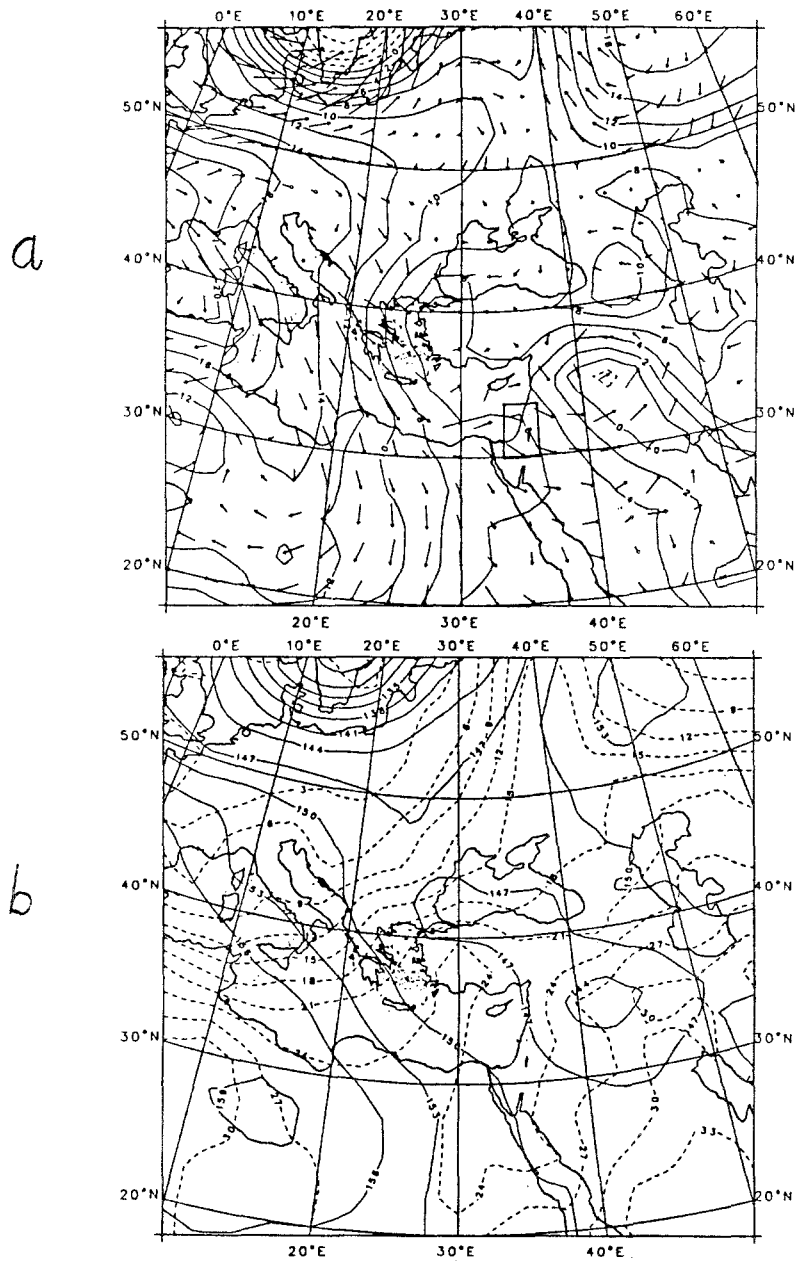

Fig. 5. The 1000 (5a) and 850 (5b) HPa ECMWF analyzed charts for the 17 June 1987 12 UTC. Wind arrows represent 12 hour displacements. Contour interval is 2 and 3 dm for (a) and (b) respectively. In (b), dashed lines are isotherms at 3°C intervals. In (a) model domain is drawn.

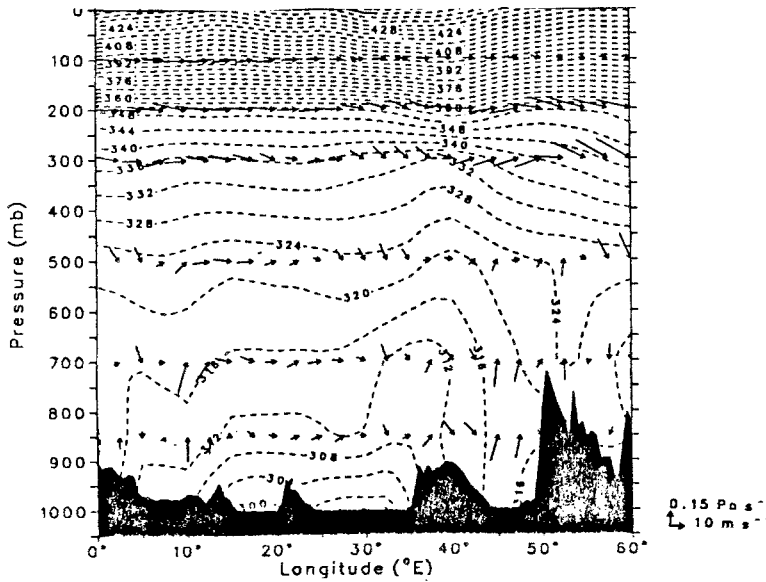

Fig. 6. The vertical cross-section along latitude 32°N of wind arrows and potential temperature on the 17 June 1987 UTC. Wind arrows represent 4 hour displacement.

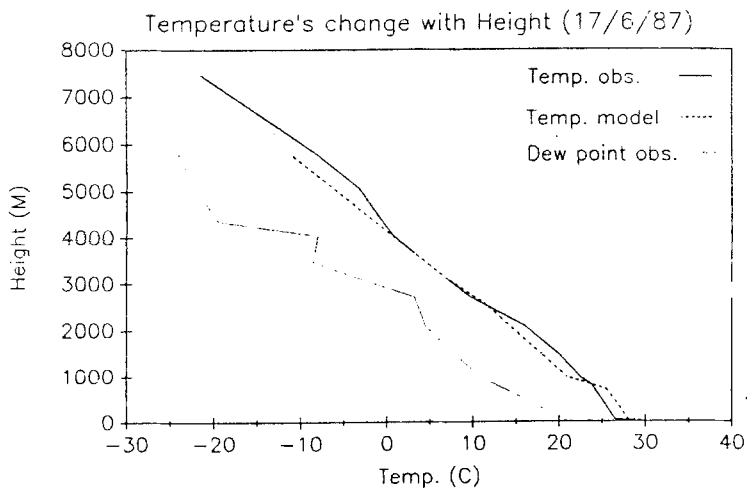

Fig. 7. The Bet-Dagan temperature (full) and dew-point profiles on 17 June 1987 12 UTC. Dashed line is the model 6 h forecast.

SB front is the anabatic flow from the Jordan Valley and Dead Sea which opposes the westerly cooler SB flow as illustrated by Alpert *et al.* (1982).

Special emphasis will be given here to the two warm thermal ridges strongly associated with the mountains oriented south to north. Reaching temperatures as high as 29°C they lead to a 925 HPa isobaric temperature gradient of about 5-6° C over a short distance of about 40-50 km and enhance the SB front (see fig. 8b). Of

particular interest and important in the contex of the PBL height, to be discussed later, notice the slight easterly downwind deviation of the thermal ridges from their probable source - the mountains. This easterly shift is more pronounced above the western ridge, where the SB strengthens the synoptic induced winds.

3.3. PBL Height Variations

The spatial cross-sectional variations of the PBL height (along y-axis point 21 in Fig. 8), are shown in Fig. 9 for four times: 08, 10, 12 (corresponding to Fig. 8) and 14 UTC. At 08 UTC, heating has just started, and the PBL height nearly follows the topography, except in the Jordan Valley between the mountain ridges where the PBL is thinner (400 m). As the SB penetrates land at 10 UTC (dashed line) and the inland convection increases, a drastic change in PBL height occurs. At the coast (point A), the PBL height dropped by 50% to 600 m, while over the mountain (point B) and the Valley (point C), the opposite happens, i.e., the PBL height increases sharply to 3000 and1500 m respectively at B and C as compared to those 2 h earlier. At 12 UTC this process continues but much more slowly as the SB front moves inland (from point X=19 to X=20), and the PBL height grows farther to the east. When the surface starts cooling, the PBL height drops through the full cross-sectional line at 14 UTC. The Mediterranean SB penetration into the valley at that time causes the PBL height drop to be particularly significant over the valley - from 3200 to 1500 m within a couple of hours. The abrupt wind increase (5 to 15 m/s) associated with this phenomenon, was discussed by Alpert *et al.* (1982).

The temporal variation at the three points A, B and C is summarized in Fig. 10. The main conclusions follow:

(i) In the coastal region (point A), the PBL height drops early in the morning as the SB penetrates while in the other regions it continues to grow with the enhanced convection.

(ii) At 1200 UTC the SB reaches the mountain top (point B), causing the PBL height to drop from 2000 to 1400 m in within one hour.

(iii) Over the Jordan Valley (point C), the PBL drop starts only after 1300 and is the sharpest as it occurs in coincidence with the reduction in daily heating.

4. Discussion and Conclusions

The depth of the mixed layer over complex topography is strongly influenced by the mesoscale circulations and their interaction with the synoptic forcing as well as the quite well-known factors over flat infinite homogeneous terrain i.e. the surface/upper-level heat fluxes, and the lapse rate. In the present paper, special emphasis is given to the interaction between the mesoscale SB circulations over topography and the large-scale forcings in two synoptic situations with reversed large-scale flow. That is the reason that we also did a 'winter case' simulation with easterly synoptic flow (not shown here). The following general conclusions from both simulations can be drawn. First, in the coastal region, the PBL is not

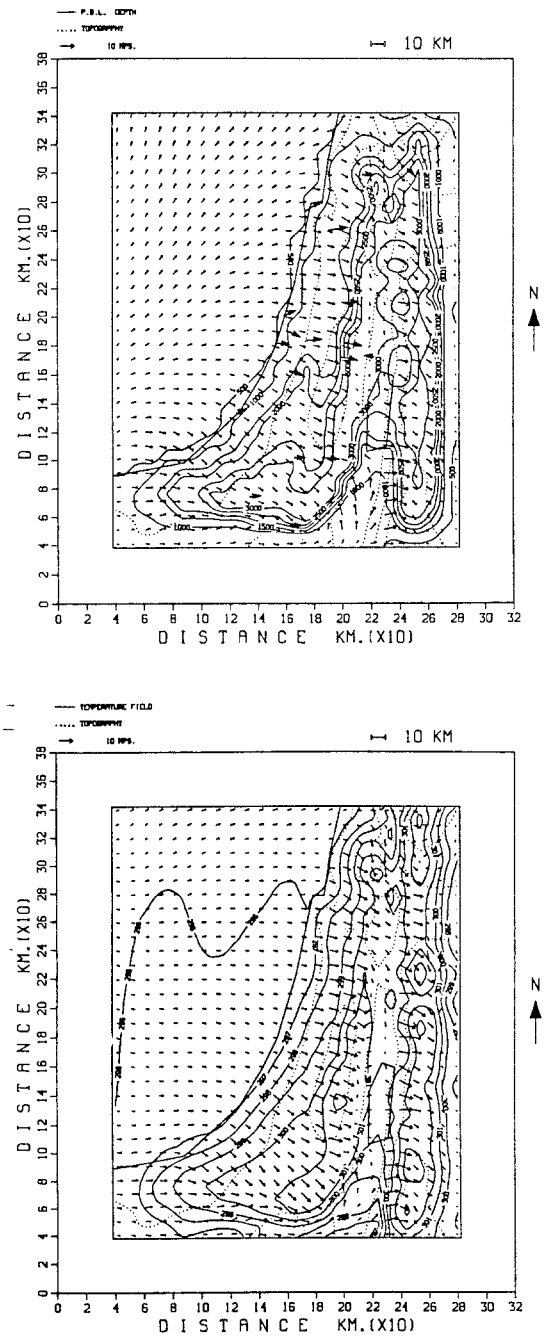

Fig. 8. (a) Model-simulated surface winds at 17 June 1987 12 UTC along with PBL height, h (full 500 m interval) and topography (dotted, 300 m interval). The observed wind vectors are also shown. (b) Model-simulated 925 HPa winds at 17 June 1987 12 UTC along with the temperature (full, 1K interval) and topography as in (a).

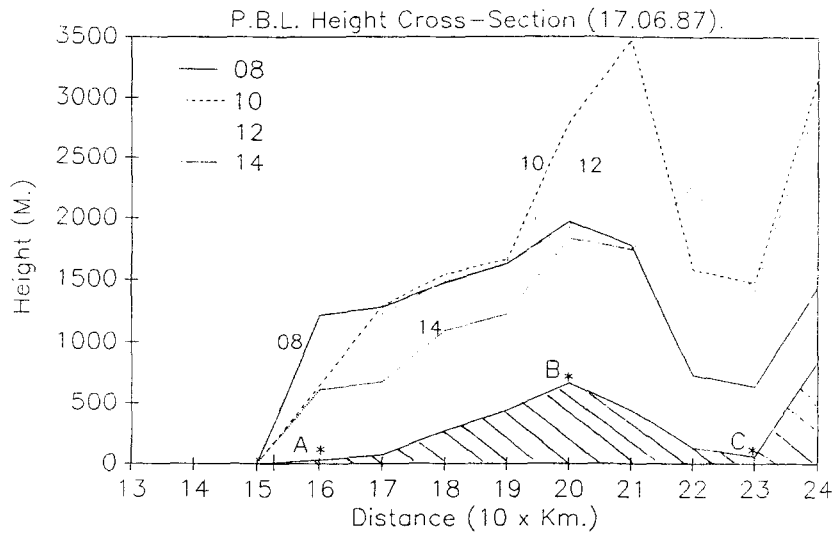

Fig. 9. The spatial cross-sectional variations of the model PBL height (m) along latitude 21 of Fig. 8 for 08 (full line), 10 (dashed), 12 (light dotted) and 14 (heavy dotted) UTC.

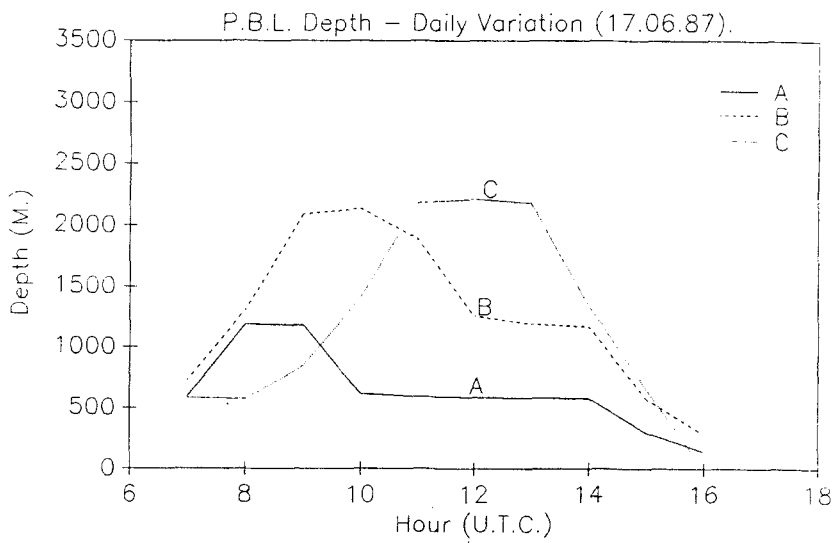

Fig. 10. The time variation of the model PBL height (m) at the three points A (full), B (dashed) and C (dotted). Location of the points is shown in Figs. 2 and 9.

as deep as it is inland and it tends to become even shallower at about 11 LST. In the inner regions the maximum PBL occurs about 3 h later. Second, the thermal ridges over the mountains become convergent lines for the horizontal flow. At the same time, being elevated mixed layers, they contribute to the sharp increase of the PBL height. The locations of the upper level thermal ridges are strongly affected by the interaction of the large-scale flow with the SB, and this becomes

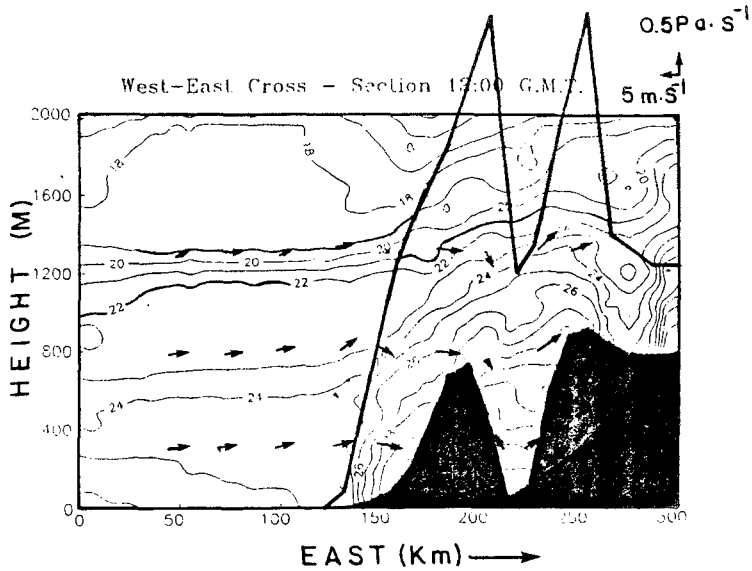

Fig. 11. the vertical cross-sections of the model simulated temperature (thin full line, 1°C interval) and wind arrows on 17 June 1987 12 UTC. Heavy full line shows the PBL height variation.

the dominant factor in determining the shift of the lines of maximum PBL height relative to the mountains. To illustrate the latter, Figs. 11 and 12 present the wind and the temperature vertical cross-sections (along the same line as in Fig. 6) during the summer and winter cases along with the PBL height at 12 UTC. These cross-sections show both the horizontal shifts of the thermal ridges relative to the mountain peaks and the associated dislocations of the PBL height.

These latter findings are strongly related to the much larger-scale effects of the elevated mixed layers due to the Rockies and the Mexican plateau on thunderstorm initiation (Benjamin and Carlson, 1986), Of course, here the horizontal scale of the effects is at least an order of magnitude smaller (10 km compared to 100 km). Another point to mention is the major effect that changes of PBL height may have on the dispersion of air-pollution. In this context we should mention recent results obtained during the recent SCCCAMP (South-Central Coast Cooperation Aerometric Monitoring Program) of lidar observations of mixing-layer over complex terrain by McElroy and Smith (1991). Their study area over southern California is very similar to that of our present work, both in the terrain and in the synoptic forcing, and their findings are also very reminiscent of ours. In particular, Fig. 13 which is Fig. 8 from McElroy and Smith (1991), shows how the mixing layer aloft generated by the mountain, strongly influences the PBL height and consequently the dispersion of air pollutants, which may be presented in such a coastal area. Fig. 13 should be compared with our simulation result in Fig. 12.

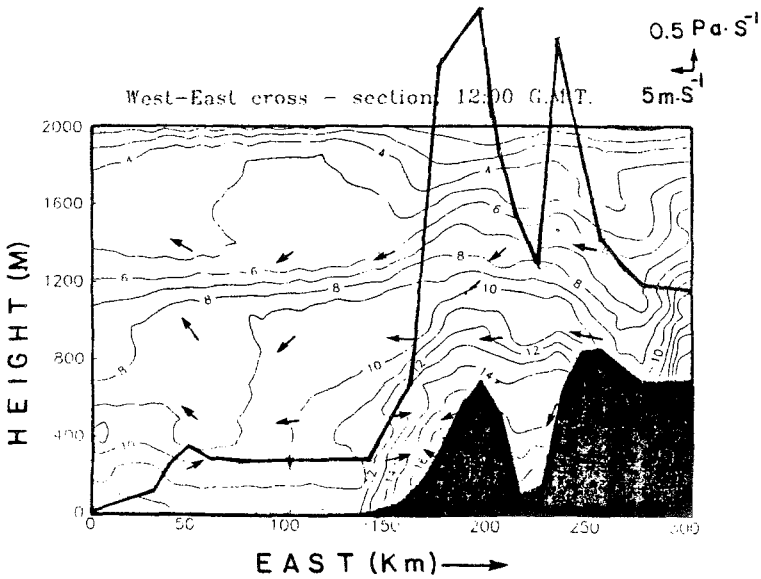

Fig. 12. As in Fig. 11 but for the winter case.

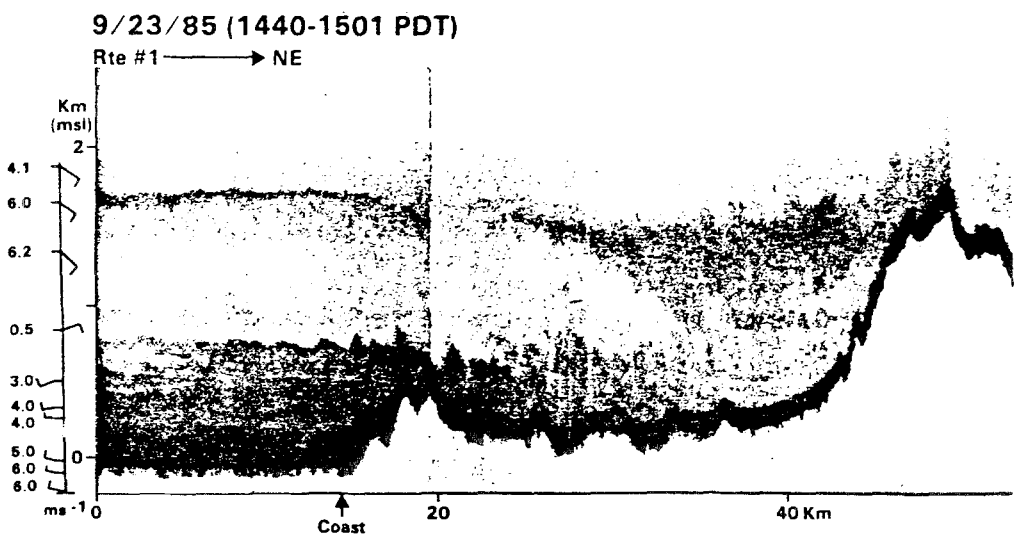

Fig. 13. Grey-scale representation of lidar backscatter signal return (at 0.532 $\bar{l}$m) for 23 September 1985, 1440-1501 PDT, with the wind sounding for station NDT (Pt. Mugo, South California) at 1459 PDT. From McElroy and Smith (1991, Fig. 8).

Acknowledgement

Support to Mr. Lieman was provided by the Israel-USA Binational Science Foundation Grant Nos. 8600230 and 8900186. Data for the model simulations is from the ECMWF and IMS (Israel Meteorological Service). Thanks to NCAR and B. Kuo for support in the adaptation of the PSU/NCAR model at TAU. Thanks to

Rachel Duani for typing and to A. Dvir for helping in drafting the figures.

References

Alpert, P., A. Cohen, J. Neuman and E. Doron, 1982. *A model simulation of the summer circulation for the Eastern Mediterranean past Lake Kinneret in the Jordan valley*. Mon. Wea. Rev. **110**, 994–1006.

Alpert, P., 1988. *The combined use of three different approaches to obtain the best estimate of meso-A surface winds over complex terrain*. Bound. Layer Meteor., **45**, 291–305.

Alpert, P. and G. Getenio, 1988. *One level modelling for diagnosing surface winds over complex terrain*. Part I: *Comparison with a 3-D modelling in Israel*. Mon. Wea. Rev. **116**, 2025–2046.

Alpert, P., B. Getenio and R. Rosental, 1988. *One level modelling for diagnosing surface winds over complex terrain*. Part II: *Applicability to short range forcasting*. Mon. Wea. Rev. **116**, 2047–2061.

Alpert, P., Abramski R. and Neeman B.U., 1991. *Persian trough or subtropical high –the prevailing summer synoptic system in Israel*. Israel J. of Earth Sci., (in press).

Anthes, R. A. and T.T. Warner, 1978: *Development of hydrodynamic models suitable for air pollution and other mesometeorological studies*. Mon. Wea. Rev., **106**, 1045–1078.

Anthes, R.A., E.-Y. Hsie and Y.-H. Kuo, 1987. Description of the Penn State/NCAR mesoscale model version (MM4)., 66 pp.

Benjamin, S.G., and T.N. Carlson, 1986. *Some effects of surface heating and topography on the regional severe storm environment*. Mon. Wea. Rev., **114**, 307–329.

Cressman, G. P., 1959. *An operative objective analysis scheme*. Mon. Wea. Rev. **87**, 367–374.

Dayan, U., R. Shenhav and M. Graber, 1988. *The spatial and temporal behavior of the mixed layer in Israel*. J. Appl. Meteor. **27**, 1382–1394.

Deardorff, J. W., 1978. *Efficient prediction of ground surface temperature and moisture with inclusion of a layer of vegetation*. J. Geophys. Res. **83**, 1889–1903.

Goodin, W.R., G.J. McRae and J.H. Seidenfeld, 1979. *A comparison of interpolation methods for sparse data: Application to wind and concentration fields*. J. Appl. Meteor., **18**, 761–771.

Haltiner G.J. and R.T. Williams, 1980. *Numerical Prediction and Dynamic Meteorology*. J. Wiley, New York, 477 pp.

Hasmonay, R., Dayan U. and Cohen A., 1991. *Lidar Observation of the atmospheric boundary layer in Jerusalem*. J. Appl. Meteor., (in press).

Lieman R., 1990. *Investigation of the mesoscale flow in the planetary boundary layer over Israel* – a numerical study. (M. Sc. thesis, in Hebrew).

McElroy J.L., and T.B. Smith, 1991. *Lidar descriptions of mixing-layer thickness characteristics in a complex terrain/coastal environment* J. Appl. Met., **30**, 585–597.

Pielke, R.A., 1984. *Mesoscale Meteorological Modelling*, Academic Press, New York, 612 pp.

Seaman N.L., F.L. Ludwig, E.G. Donall, T.T. Warner and C. M. Bhumralkar, 1989. *Numerical studies of urban planetary layer structure under realistic synoptic conditions*. J. Appl. Met. **28**, 760–781.

Segal, M., Y. Mahrer and R. A. Pielke, 1982. *Application of a numerical mesoscale model for the evaluation of seasonal persistent regional climatological patterns*. J. Appl. Meteor., **21**, 1754–1762.

Segal, M., Y. Mahrer, R.A. Pielke and R.C. Kessler, 1985. *Model evaluation of the summer daytime induced flows over southern Israel*. Isr. J. Earth. Sci., **34**, 39–46.

Stull, R.B., 1988. *An introduction to boundary layer meteorology*, Kluwer publ. 666 pp.

Young, G. S. and R. A. Pielke, 1983. *Application of terrain height variance to Mesoscale Modelling*. J. Atmos Sci., **40**, 2555–2560.

Zhang. D. and R. A. Anthes, 1982. *A high resolution model of the planetary boundary layer. Sensitivity tests and comparisons with the SESAME-79 data*. J. Appl. Meteor., **21**, 1594–1609.